Apoptosis (2015) 20:1307–1320
DOI 10.1007/s10495-015-1151-z

ORIGINAL PAPER

A modified thymosin alpha 1 inhibits the growth of breast cancer both in vitro and in vivo: suppressment of cell proliferation, inducible cell apoptosis and enhancement of targeted anticancer effects

Xingzhen Lao[1] · Bin Li[1] · Meng Liu[1] · Chen Shen[1] · Tingting Yu[1] · Xiangdong Gao[1] · Heng Zheng[1]

Published online: 18 August 2015
© Springer Science+Business Media New York 2015

Abstract Thymosin alpha 1 (Tα1) is commonly used for treating several diseases; however its usage has been limited because of poor penetration of the target tissue, such as tumor cells. In the present study, Tα1-iRGD, a peptide by conjugating Tα1 with the iRGD fragment, was evaluated its performance in MCF-7 and MDA-MB-231 human breast cancer cells. Compared with the wild-type peptide, Tα1-iRGD was more selective in binding tumor cells in the cell attachment assay. Furthermore, the MTT assay confirmed that Tα1-iRGD proved more effective in significantly inhibiting the growth of MCF-7 cells in contrast to the general inhibition displayed by Tα1. Further, conjugation of Tα1 with iRGD preserved the immunomodulatory activity of the drug by increasing the proliferation of mouse spleen lymphocytes. Further, compared with Tα1 treatment, Tα1-iRGD treatment of MCF-7 cells considerably increased the number of cells undergoing apoptosis, resulting in a dose-dependent inhibition of cancer cell growth, which was associated with a much better effect on up-regulation of the expression of BCL2-associated X protein (*Bax*), *caspase 9*, etc. More importantly, treatment with Ta1-iRGD was more efficacious than treatment with Ta1 in vivo. This study highlights the importance of iRGD on enhancement of cell penetration and tumor accumulation. In summary, our findings demonstrate that the novel modified Tα1 developed in this study has the potential to be used for treating breast cancer.

Keywords RGD · Tumor homing · Apoptosis

✉ Xiangdong Gao
xdgao@cpu.edu.cn

✉ Heng Zheng
cpu_zhengheng@163.com

Xingzhen Lao
lao@cpu.edu.cn

Bin Li
1libin@163.com

Meng Liu
mytt@live.cn

Chen Shen
pharma_sc@163.com

Tingting Yu
ting15215487519@163.com

[1] School of Life Science and Technology, China Pharmaceutical University, 24 Tongjiaxiang, Nanjing 210009, People's Republic of China

Introduction

Thymosin alpha 1 (Tα1) is a 28-amino acid immunomodulating peptide derived from prothymosin alpha in the thymus [1]. Tα1 has been broadly used in the treatment of various diseases, including immune deficiencies [2], infectious diseases [3–5] and cancers [6, 7]. However, use of Tα1 as an anticancer drug in clinical trials has been limited because of its poor tumor penetration; therefore, Tα1 was previously used only as a complementary agent with cytokines and chemotherapeutic agents [8–11].

The iRGD fragment [12, 13] has a unique advantage that it penetrates tumor cells because of its highly selective affinity to neurophilin-1 and αv integrins [12, 14, 15] that are highly expressed in many tumor cell types but not in normal tissues. Therefore, the iRGD fragment has been utilised as a powerful cyclic tumor-homing and tumor-penetrating peptide. The iRGD fragment specifically binds to αv integrins at first, following which it is proteolytically cleaved to CRGDK/R, thus activating a neuropilin-1 (NRP-1)-

dependent C-end Rule (CendR) sequence (R/KXXR/K) internalisation pathway to achieve cell internalisation and tumor penetration [16, 17].

Based on the previous study, Tα1-iRGD, a peptide in which the iRGD fragment (CRGDKGPDC) was introduced into the C-terminus of Tα1 by conjugating them with a linker (GGGG) [18], was further studied its activity in inhibiting the growth of the human breast cancer cell line MCF-7. Moreover, we further explore the tumor targeting effect of Tα1-iRGD by in vitro MCF-7 model and in vivo MCF-7 breast tumor-bearing nude mice model, which might illustrate the real biologic mechanism of iRGD on enhancement of targeted anticancer effects of Tα1-iRGD both in vivo and in vitro.

Materials and methods

Materials

MCF-7 and MDA-MB-231 human breast cancer cell line was purchased from American Type Cell Culture (ATCC, Shanghai, China). Concanavalin A (ConA) was purchased from Sigma-Aldrich (USA). Paclitaxel (Taxol) was provided by Jiangsu Yew Pharmaceutical Co., Ltd. (Wuxi, Jiangsu Province of China). Tα1-iRGD, Tα1 and their FITC-labelling peptides were synthesized by ChinaPeptides Company Limited (Shanghai, China). ICR mice (SPF) were purchased from the Comparative Medicine Center of Yangzhou University, China. Balb/c nude mice were purchased from the Changzhou Cavens laboratory animal Co. Ltd. (Changzhou, China). Anti-Caspase-9 antibody (ab32539) were purchased from Abcam. All experimental procedures using animals used in the our study were performed in strict accordance with the interdisciplinary principles and guidelines for the use of animals in research and was approved by Jiangsu Provincial Experimental Animal Management Committee under Contract 2012(su)-0035.

Methods

Cell proliferation assay

MCF-7 or MDA-MB-231 cells were maintained in RPMI 1640 supplemented with 10 % (v/v) foetal bovine serum (FBS), 100 U/mL penicillin and 100 μg/mL streptomycin. MCF-7 or MDA-MB-231 cells were seeded in 96-well plates at a density of 5000 cells/well for 6 h and then incubated with serial dilutions of Tα1 or Tα1-iRGD at 37 °C at a final volume of 200 μL for 36 h. Paclitaxel (0.0125 μmol/mL) and RPMI 1640 were used as the positive and negative controls, respectively. Cell proliferation was then measured using the MTT assay as described previously [19]. In brief, MTT solution (20 μL, 5 g/L) was added to each well and incubated at 37 °C for 4 h. Subsequently, the medium was removed and 150 μL DMSO was added to each well to dissolve the resulting formazan precipitate. Absorbance was determined at 570 nm using a microplate reader. After the first round of treatment, another round of treatment with Tα1 or Tα1-iRGD at lower concentrations was conducted. The relative inhibition of cell proliferation (%) was calculated by the equation $(A_N - A_T)/A_N \times 100$ %, where A_T refers to absorbance of the treatment group and A_N refers to absorbance of the negative control group. Cell viability was calculated as CV = (absorbance of the treatment group/absorbance of the negative control group) × 100 %.

Cell attachment assay

The cell attachment assay was performed as described previously [20]. In brief, several diluted concentrations of Tα1 or Tα1-iRGD were coated onto a 96-well ELISA plate (Costar, USA) at 4 °C overnight. Wells coated with phosphate-buffered saline (PBS) were used as the negative control. Each well in the plate was blocked using 2 % bovine serum albumin in RPMI 1640 at 37 °C for 2 h. The plate was then washed 3 times with isotonic buffered saline prior to seeding 100 μL of MCF-7 cells (3×10^4 cells/well) and then incubated for 1 h at 37 °C. Subsequently, the plate was washed 3 times with isotonic buffered saline to wash away non-adherent cells. The adherent cells in each well were fixed in PBS containing 3 % paraformaldehyde and 2 % saccharine, stained with 0.5 % crystal violet staining buffer, examined by phase-contrast microscopy and documented by taking pictures. Subsequently, the crystal violet in the adherent cells was extracted with 10 % acetic acid (100 μL per well) and the plates were read using a microplate reader at 595 nm. The relative cell adhesion (%) was calculated using the formula $(A_T - A_C)/A_C \times 100$ % (where A_T refers to absorbance of the treatment group and A_C refers to absorbance of the negative control group).

Spleen lymphocyte proliferation assay

Suspensions of single spleen cells were prepared from ICR mice as described previously [21]. Subsequently, the cells were resuspended in RPMI 1640 containing 10 % FBS at a final concentration of 2×10^6 cells/mL. Different concentrations of Tα1 or Tα1-iRGD were added and co-incubated with ConA (5 μg/mL) at 37 °C for 36 h. ConA (5 μg/mL) and RPMI 1640 were used as the negative and normal controls, respectively. Further, the effect on

proliferation was determined using the MTT assay as described above.

Apoptotic assay

The apoptotic assay was performed as described previously [22, 23]. In brief, a suspension of MCF-7 cell was prepared using 0.25 % trypsin, and the cells were seeded in a 6-well plate at an initial density of 4×10^4 cells/well and incubated in a humidified atmosphere of 5 % CO_2 and air at 37 °C for 6 h. Tα1 or Tα1-iRGD at a concentration of 0.02 μmol/mL were then added to the wells and incubated for 36 h. RPMI 1640 was used as the negative control. Following drug treatment, the cells were trypsinised (0.25 % trypsin) and washed twice with cold PBS. For each sample, 10^5 cells were counted and resuspended in a binding buffer, followed by incubation with 5 μL of Annexin V-FITC and 5 μL of propidium iodide for 15 min, according to the manufacturer's protocol manual (Annexin V-FITC and PI Apoptosis Kit, Biouniquer, Nanjing, China). Apoptotic cells were determined using a FACScan flow cytometer (BD Biosciences).

Semi-quantitative reverse transcription-polymerase chain reaction (RT-PCR) and Western blot analysis

Semi-quantitative RT-PCR was performed as described previously [24]. In brief, following 36 h of treatment, total cellular RNA was obtained by TransZol (Beijing TransGen Biotech Co., Ltd., China) and 1 μg of RNA was reverse transcribed to cDNA using TransScript First-Strand cDNA Synthesis SuperMix kit according to the manufacturer's instructions (Beijing TransGen Biotech Co., Ltd., China). These cDNAs were then amplified using PCR; the products were separated by 2.0 % agarose gel electrophoresis, stained with ethidium bromide and visualised under ultraviolet light using a gel imaging system. The RT-PCR exponential phase was set from 25 to 35 cycles to allow sufficient semi-quantitative comparisons among cDNAs developed from different treatments. Each PCR regime involved an initial 5-min denaturation step at 94 °C, followed by 34 amplification cycles at 94 °C for 30 s, 51–57 °C for 30 s [55 °C for BCL2-associated X protein (*Bax*) and glyceraldehyde-3-phosphate dehydrogenase (*GAPDH*), 51.5 °C for *caspase 9* and 57 °C for *caspase 3*] and final extension at 72 °C for 5 min. The following primers were used: Bax forward primer: 5′-TCCCCCCGA GAGGTCTTTTTC-3′ and Bax reverse primer: 5′-TCCCGGAGGAAGTCCAATGTC-3′; caspase 9, apoptosis-related cysteine peptidase (*CASP9*) forward primer: 5′-ATCAACAATGTGAACTTCTGC-3′ and *CASP9* reverse primer: 5′-GATGTTCACAATCTTCTCGAC-3′; *caspase 3*, apoptosis-related cysteine peptidase (*CASP3*) forward primer: 5′-GAACTGGACTGTGGCATTGAG-3′ and *CASP3* reverse primer: 5′-CACAAAGCGACTGGAT GAACC-3′ and *GAPDH* forward primer: 5′-GGGAGC CAAAAGGGTCATCAT-3′ and *GAPDH* reverse primer: 5′-CAGGGGTGCTAAGCAGTTGGT-3′. The predicted lengths of the RT-PCR products were 179 bp (*Bax*), 303 bp (*CASP9*), 163 bp (*CASP3*) and 139 bp (*GAPDH*). The intensities of the cDNA bands for each treatment were normalised to the *GAPDH* band intensities. Western blot analysis was also performed according to standard procedures based on the result of RT-PCR.In brief, cells were lysed and the protein was subjected to SDS-PAGE and further transfer to PVDF Western blotting membranes and finally identified by primary antibodies and species-specific horseradish peroxidise(HRP) conjugated secondary antibody. Chemiluminescent detection was achieved with Thermo Scientific ECL reagent.

Location of polypeptides in cells

The breast cancer cell line MCF-7 was cocultured with 200 μL FITC-labelled Tα1-iRGD and Tα1 at 0.1 mg/ml for 2 h, respectively. After being washed with PBS, the cells were incubated with Dil for 20 min at room temperature to stain the cell membrane. After being washed again,the cells were then incubated with Hoechst33342 for 10 min at room temperature to stain the cell nuclei and finally observed at inverted fluorescence Microscope (Axio Vert.A1, Carl Zeiss, Germany).

Human breast tumor model and therapy

MCF-7 breast tumors were created by implanting subcutaneously (s.c.) 1×10^7 cells into female nude mice at the age of 4–6 weeks. When the average tumor volume reached 100 mm^3, the mice were randomly divided into four groups with eight mice per group. For in vivo tumor treatment studies, group1 were subcutaneously injected with Tα1-iRGD at a dose of 0.08 μmol/kg once daily for 11 days at a site distant from the tumor, and group 2 received Tα1 at the same dose of 0.08 μmol/kg once daily. Group 3 was subcutaneously injected with 0.1 mL PBS once daily and set as a negative control. Group 4 was treated with 10 mg/kg Paclitaxel at a dose of 10 mg/kg once every 3 days and set as a positive control. The tumor volume was monitored every other day and determined using the following formula: tumor volume $= (A^2 \times B)/2$, where A is the smallest and B is the largest tumor diameters.

Histochemistry and immunohistochemistry

Hematoxylin and eosin (H&E) staining was use to detect necrosis in tumor tissues as previously described [25].

Briefly, staining for H&E was performed through standard histological procedures. Immunohistochemical staining of CD31 was used to evaluate vascular structures in the tumor tissues. Briefly, the tumors sections, 4 μm thick, were put on a coated glass slide and fixed. Sections were incubated for 18 min with H_2O_2 (3 %) for blocking endogenous peroxidase activity. Subsequently, the sections were incubated with the primary antibodies and the secondary antibody. The primary antibodies were rat anti-mouse CD31 monoclonal antibody. The secondary antibody was HRP-tagged rabbit anti-rat IgG. Finally, tissue sections were treated with 3,3-diaminobenzidine (DAB) and counterstained with hematoxylin and examined by a microscope.

Tumor targeting

To elucidate the tumor targeting of Ta1-iRGD in nude mice bearing tumor, MCF-7 tumor-bearing mice were injected via the tail vein with FITC-labelled polypeptides (0.8 mmol/L, 200 μL volumes) as previously described [26]. 2 h after the injection, the tumors, hearts, livers, spleens, lungs, and kidneys were took from nude mice for further green fluorescence detection under an in vivo Imaging System Fx Pro (Carestream, American).

Three-dimensional (3D) modeling

According to previous studies [13, 16, 17], the iRGD motif is capable of tumor-homing by initially binding to αV integrins that are specifically expressed on many tumors. The iRGD motif is subsequently cleaved by a protease to expose an internal R/KXXR/K motif, which belongs to a class of CendR peptides. The CendR peptides demonstrate proven capabilities of binding NRP-1, leading to cellular internalisation and penetration. Based on this theory, the Tα1-iRGD should be cleaved to Tα1-CRGDK, which is composed of Tα1, a linker (GGGG) and CRGDK that belongs to a class of CendR peptides. We have previously used computational approaches to model the interaction between Tα1-iRGD and integrin αvβ3 [18]. In the present study, we applied the same computational modelling approach to explore whether NRP-1 can bind Tα1-CRGDK. The structure of Tα1-CRGDK was first built by homology modelling (DS software, Accelrys Inc., USA), using the structure of Tα1 (PDB:2L9I) as the homologous template [27]. Then, the initial model was minimised using 2000 steepest descent steps and 2000 conjugate gradient steps under the CHARMmH force field. The final Tα1-CRGDK model, as a ligand, was docked with NRP-1 (PDB:3I97) [28] using the ZDOCK program [29], and the result was analysed using Molecular Operating Environment software.

Results

Tα1-iRGD increased the inhibition of MCF-7 and MDA-MB-231 cell proliferation in vitro

We performed the MTT assay to determine whether Tα1-iRGD was more effective in inhibiting the growth of MCF-7 cells than Tα1. After the first round of treatment, when MCF-7 cells were treated with various concentrations of Tα1 or Tα1-iRGD (from 0.03125 to 0.5000 μmol/mL) for 36 h, Tα1-iRGD exhibited significantly higher antiproliferative activity than Tα1 at all concentrations ($p < 0.01$) (Fig. 1a). For example, Tα1-iRGD produced a 51.5 % inhibition in the proliferation of MCF-7 cells at a concentration of 0.03125 μmol/mL, whereas Tα1 resulted in only 23.8 % inhibition at the same concentration ($p < 0.01$).

A subsequent round of drug treatment was conducted to further examine the activity of Tα1-iRGD or Tα1 at lower concentrations, and the inhibition rate of MCF-7 cells was examined (Fig. 1b). We observed that Tα1-iRGD exhibited significant antiproliferative activity even at very low concentrations when compared with Tα1. For example, 0.02 μmol/mL of Tα1-iRGD significantly inhibited cell proliferation (the rate of inhibition was 49.6 %), whereas the same concentration of Tα1 showed only slight antitumor effects, with only 2.8 % inhibition of cell proliferation ($p < 0.01$). In another experiment, 0.004 μmol/mL of Tα1-iRGD inhibited cell proliferation by 37.8 %, whereas Tα1 demonstrated only 0.64 % inhibition at the same concentration ($p < 0.001$). These results showed that Tα1-iRGD was more effective in inhibiting the growth of MCF-7 cells than Tα1. Similar results were obtained in MDA-MB-231 breast cancer cells (Fig. 1c). ER (+) MCF-7 and ER (−) MDA-MB-231 breast cancer cells are all highly express NRP1 [30, 31]. As observed in Fig. 1c, Ta1-iRGD was more effective than Ta1 in inhibiting MDA-MB-231 breast cancer cells growth. For example, 0.03125 μmol/mL of Tα1-iRGD significantly inhibited cell proliferation (the rate of inhibition was 44.6 %), whereas the same concentration of Tα1 showed only slight antitumor effects, with only 9.0 % inhibition of cell proliferation ($p < 0.05$). These results further confirmed that the addition of the iRGD fragment considerably increased the antiproliferative activity of Tα1 against breast cancer cells.

Tα1-iRGD increased MCF-7 cell attachment in vitro

After comparing the activity of Tα1-iRGD and Tα1 by the cell attachment assay in vitro, several diluted concentrations of Tα1 or Tα1-iRGD were added to ELISA plates. The results are shown in Fig. 2a, b. Compared with Tα1,

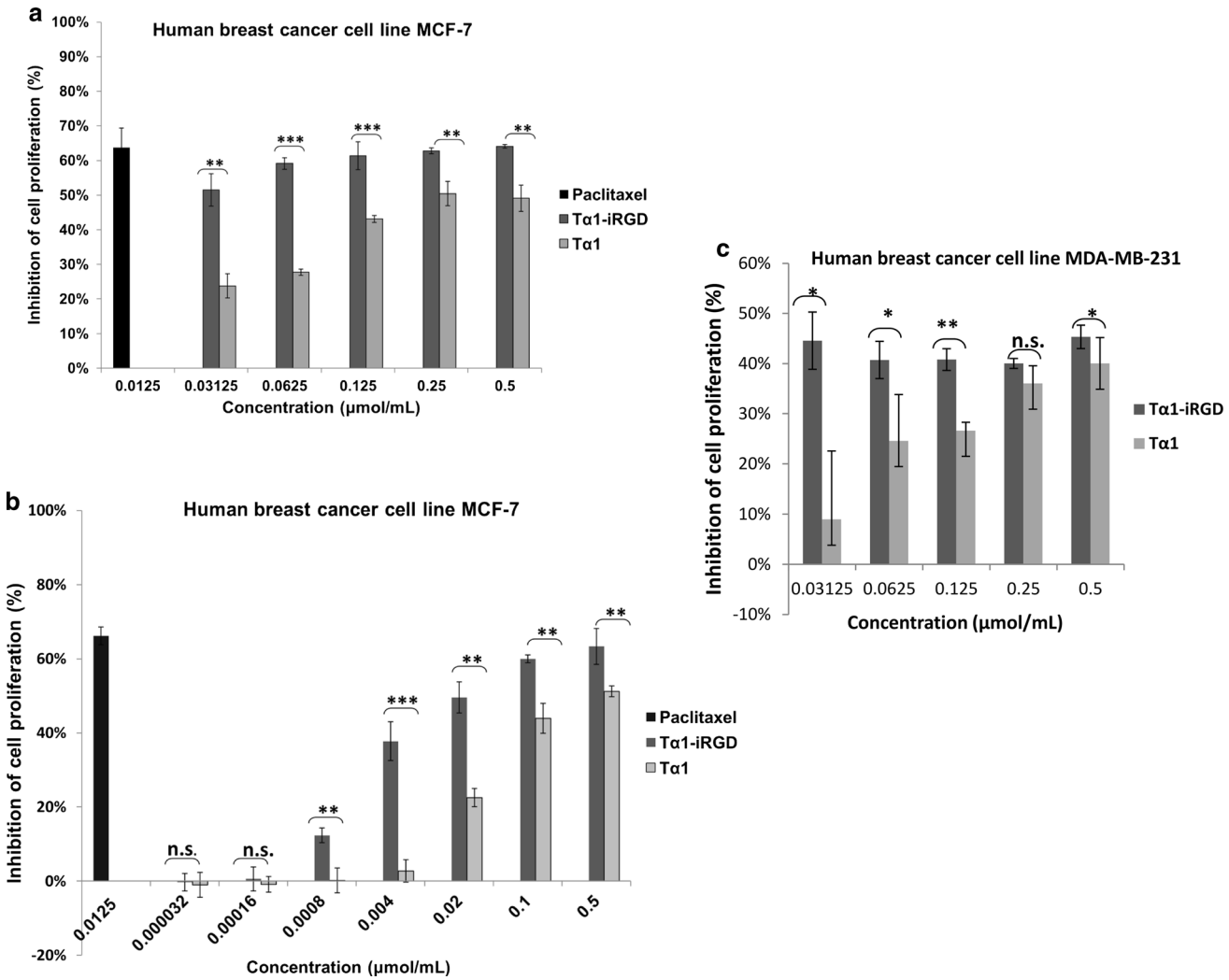

Fig. 1 Inhibition of MCF-7 and MDA-MB-231 cell proliferation by Tα1 or Tα1-iRGD. The cell suspension was incubated with Tα1 or Tα1-iRGD for 36 h and cell growth was analysed by the MTT assay. **a** Concentrations range from 0.03125 to 0.5000 μmol/mL(MCF-7). **b** Concentrations range from 0.000032 to 0.5000 μmol/mL(MCF-7). Paclitaxel (0.0125 μmol/mL) was used as the positive control and RPMI 1640 as the negative control. **c** concentrations range from 0.03125 to 0.5000 μmol/mL(MDA-MB-231). All data were expressed as the mean ± SD, n = 4. Statistical analyses were performed with Student's *t* test, *n.s.* not significant; *$p < 0.05$; **$p < 0.01$; ***$p < 0.001$

Tα1-iRGD significantly enhanced the attachment of MCF-7 cells in a concentration-dependent manner, particularly at a concentration above 0.04 μmol/mL ($p < 0.01$). Thus, these results implied a role for Tα1-iRGD in supporting MCF-7 cell attachment, primarily because of the iRGD sequence itself.

Tα1-iRGD and Tα1 produced a similar effect on the proliferation of spleen lymphocytes in vitro

The proliferation of spleen lymphocytes obtained from ICR mice was examined in vitro following treatment with different concentrations of Tα1 or Tα1-iRGD using ConA as a co-stimulant. Tα1-iRGD promoted the proliferation of mouse spleen lymphocytes in a manner similar to Tα1 (Fig. 3). No significant difference was observed in the dose-dependent proliferation of spleen lymphocytes stimulated by Tα1-iRGD and Tα1 ($p > 0.05$). Therefore, the results of these proliferation assays further suggested that the addition of iRGD to the C-terminus of Tα1 did not influence its spleen lymphocyte proliferation activity.

Tα1-iRGD displayed increased apoptotic function relative to Tα1 in MCF-7 cells

MCF-7 cells treated with Tα1 or Tα1-iRGD for 36 h showed characteristics typically associated with apoptotic changes, including marked morphological changes along

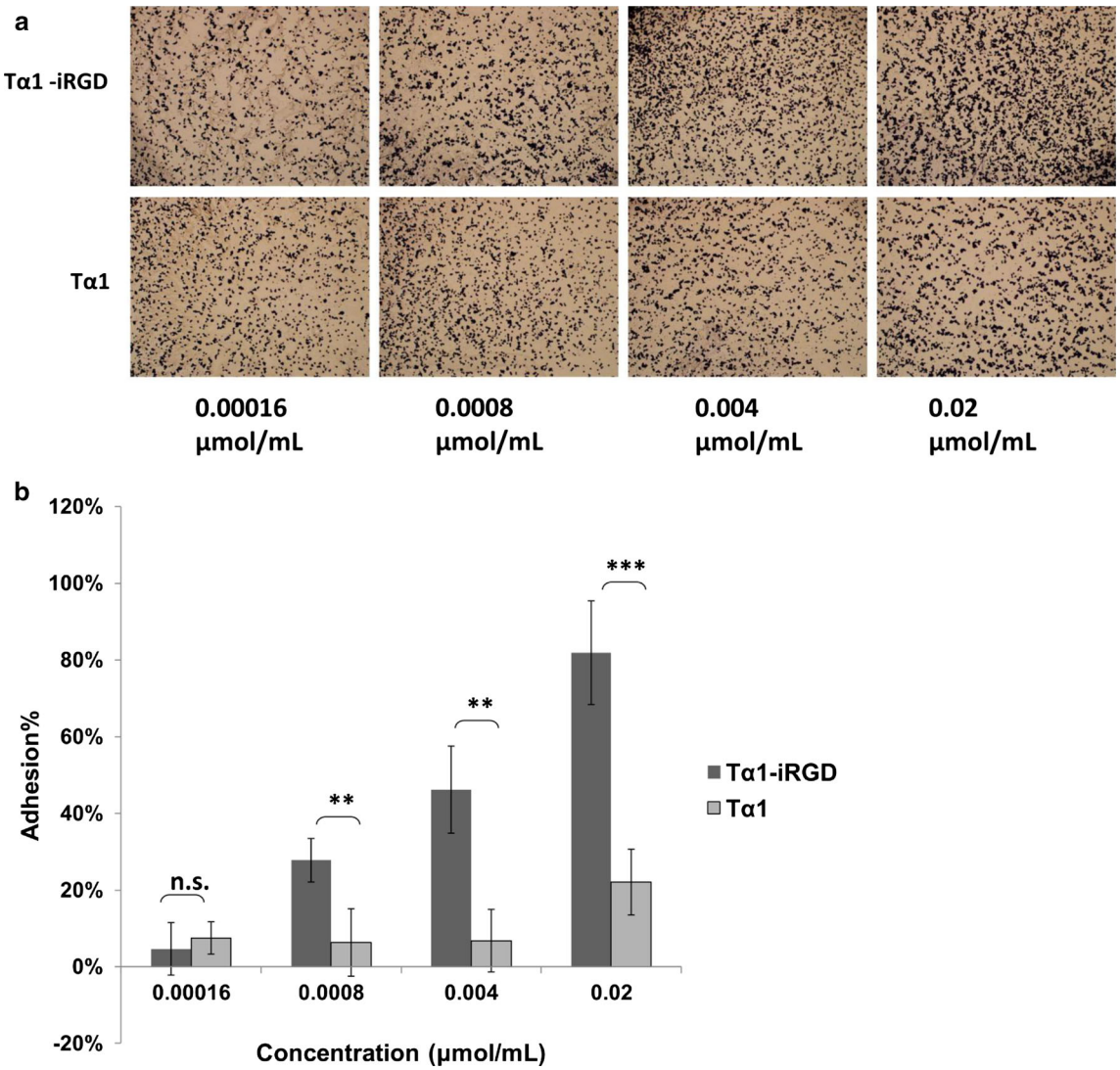

Fig. 2 Enhanced cell attachment following the conjugation of iRGD to the C-terminus of Tα1. **a** Cells bound to the wells were fixed, stained with 0.5 % crystal violet staining buffer and photographed. **b** Crystal violet was extracted and the remaining adherent human breast cancer cells were documented by a microplate spectrophotometer at a wavelength of 595 nm. All data are expressed as the mean ± SD, n = 3. Statistical analyses were performed with Student's *t* test, *n.s.* not significant; *$p < 0.05$; **$p < 0.01$; ***$p < 0.001$

with cell contraction (Fig. 4a). The apoptosis rate following Tα1 or Tα1-iRGD treatment was further verified by Annexin V-FITC/PI double staining and detected by flow cytometry. The loss of phospholipid asymmetry in the cell membrane is one of the morphological changes associated with apoptosis. During the early stage of apoptosis, phosphatidylserine, which exists only in the inner layer of the plasma membrane of live cells, translocates to the outer layer of the plasma membrane. The exposed phosphatidylserine on the surface of the plasma membrane can bind to Annexin V-FITC, and the apoptotic cells can be detected by flow cytometry following Annexin V-FITC/PI double staining. The apoptotic cells were gated into the lower right (LR) and upper right (UR) quadrants by flow cytometry; the Annexin V-positive/PI-negative cells (LR) were defined as early apoptotic, and Annexin V-positive/PI-positive cells (UR) were considered as late apoptotic. The quadrants of Annexin V-negative/PI-negative cells (lower left. LL,) and Annexin V-negative/PI-positive cells (upper left, UL) were considered as live cells and necrotic cells, respectively. The total percentages in the LR and UR quadrants were computed as the extent of apoptosis in our data analysis.

Following Tα1 or Tα1-iRGD (0.02 μmol/mL) treatment for 36 h, as described in Fig. 4b, Tα1-iRGD was significantly more effective in inducing apoptosis in MCF-7 cells than Tα1 ($p < 0.05$). The total apoptotic population induced by Tα1-iRGD increased up to 15.22 % (7.62 %

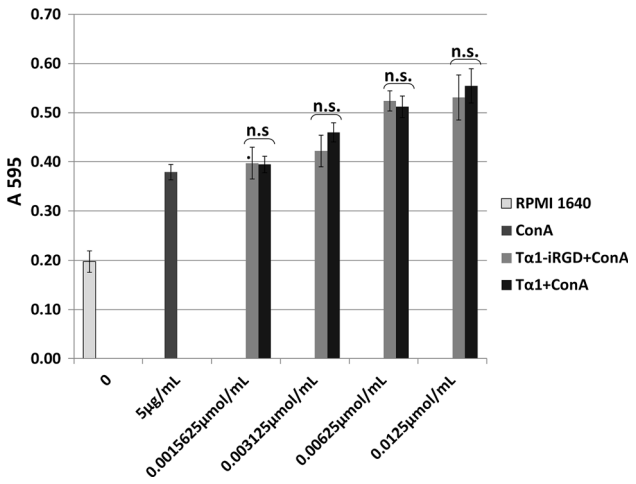

Fig. 3 Tα1-iRGD and Tα1 displayed similar spleen lymphocyte proliferation activities. Spleen lymphocytes were treated with Tα1-iRGD and Tα1. RPMI 1640 was used as the normal control, and ConA (5 μg/mL) was used as the negative control. ConA (5 μg/mL) was also used as a co-stimulant with different concentrations of Tα1-iRGD or Tα1. All data are expressed as the mean ± SD, n = 4. Statistical analyses were performed with Student's *t* test, *n.s.* not significant; *p < 0.05; **p < 0.01; ***p < 0.001

early apoptotic plus 7.60 % late apoptotic, Fig. 4c), whereas that induced by Tα1 reached up to 6.31 % (3.42 % early apoptotic plus 2.89 % late apoptotic, Fig. 4c). In conclusion, this apoptotic assay further confirmed that the addition of iRGD to the C-terminus of Tα1 increased its apoptotic function relative to Tα1 in MCF-7 cells.

Tα1-iRGD increased the expression of genes associated with apoptosis in MCF-7 cells compared with Tα1

Several previous studies have implicated *Bax* as an essential gateway in drug-induced apoptotic signalling pathways. *Bax* releases cytochrome C from mitochondria and activates subsequent downstream effecter caspases, eventually leading to progressive caspase-independent mitochondrial dysfunction and cell death [32, 33]. *CASP9* [34, 35] and *CASP3* [36] also play distinct roles during the apoptotic process.

We performed semi-quantitative RT-PCR to further emphasise the possibility and level of expression of *Bax*, *CASP9* and *CASP3* in MCF-7 cells under different treatment conditions. Total cellular RNA was extracted and cDNA synthesised using standard methods. Densitometric analysis showed that *Bax* mRNA expression in MCF-7 cells was significantly higher following Tα1-iRGD treatment (mRNA: 0.143 ± 0.013) than after Tα1 treatment (mRNA: 0.013 ± 0.007) (Fig. 5a). In addition, both *CASP9* mRNA expression (0.117 ± 0.013 vs. 0.003 ± 0.005) and *CASP3* mRNA expression (0.687 ± 0.114 vs. 0.282 ± 0.013) were significantly higher after Tα1-iRGD treatment than after Tα1 treatment. The result clearly demonstrated that early *Bax* activation plays a critical role in Tα1-iRGD or Tα1-induced apoptosis signalling. Specifically, Tα1-iRGD can induce a higher expression of *Bax* than Tα1, consequently resulting in a higher expression of *CASP9* and *CASP3*. These data may illustrate why Tα1-iRGD displayed a better effect on inducing breast cancer cell apoptosis than Tα1.

Consistent with these results, Tα1-iRGD treatment resulted in better effect on triggering activation of Caspase 9 than Tα1-iRGD treatment (Fig. 5b) in Western blot analysis. In addition,densitometric analysis showed that Caspase 9 (0.842 ± 0.052 vs. 0.478 ± 0.100) were significantly higher after Tα1-iRGD treatment than after Tα1 treatment.

Tα1-iRGD penetrate into cells

The distribution of Tα1-iRGD or Tα1 in cells was traced by FITC-labelling. When the treated cells were observed inverted fluorescence microscope after 2 h of incubation, Tα1 was located on cell membrane (Fig. 6a), whereas Tα1-iRGD entered into cytoplasm and even nuclei (Fig. 6b). It indicated that conjugation of iRGD with the Tα1 C-terminus is able to penetrate cell membrane with some extends.

Tα1-iRGD exhibits a better tumor growth inhibitory effect than Ta1 on human breast tumor xenografts

To assess the antitumor effect of Tα1-iRGD, the mice bearing MCF-7 breast tumor Xenografts were treated with the direct s.c. administration of Tα1-iRGD, Ta1. As shown in Fig. 7, the tumor growth inhibition seen with Tα1-iRGD was better (day 11) than that was seen with Tα1. More importantly, Tα1-iRGD treatment resulted in significant inhibition of tumor growth at a dose ($p < 0.001$, day 11) at which Tα1 showed no significant effect. The tumor growth inhibition seen with Tα1-iRGD was nearly similar with that of paclitaxel. Therapeutic effects on tumor growth were calculated as $(1 - T/C) \times 100$ %, where A is mean treated tumor volume and C is mean control tumor volume. In comparison, Tα1-iRGD inhibited tumor growth by (45.94 %) at day 11 (Fig. 7b), while Tα1 inhibited tumor growth only by 24.22 %. Therefore, Tα1-iRGD was more effective than Tα1 in inhibiting MCF-7 breast tumor growth in vivo,indicating the efficacy of iRGD-mediated drug delivery.

Ta1-iRGD decreased vascular structures in the tumor tissues

Necrosis in tumor tissues was detected by H&E staining. As shown in Fig. 8a, comparing with the Tα1 treatment

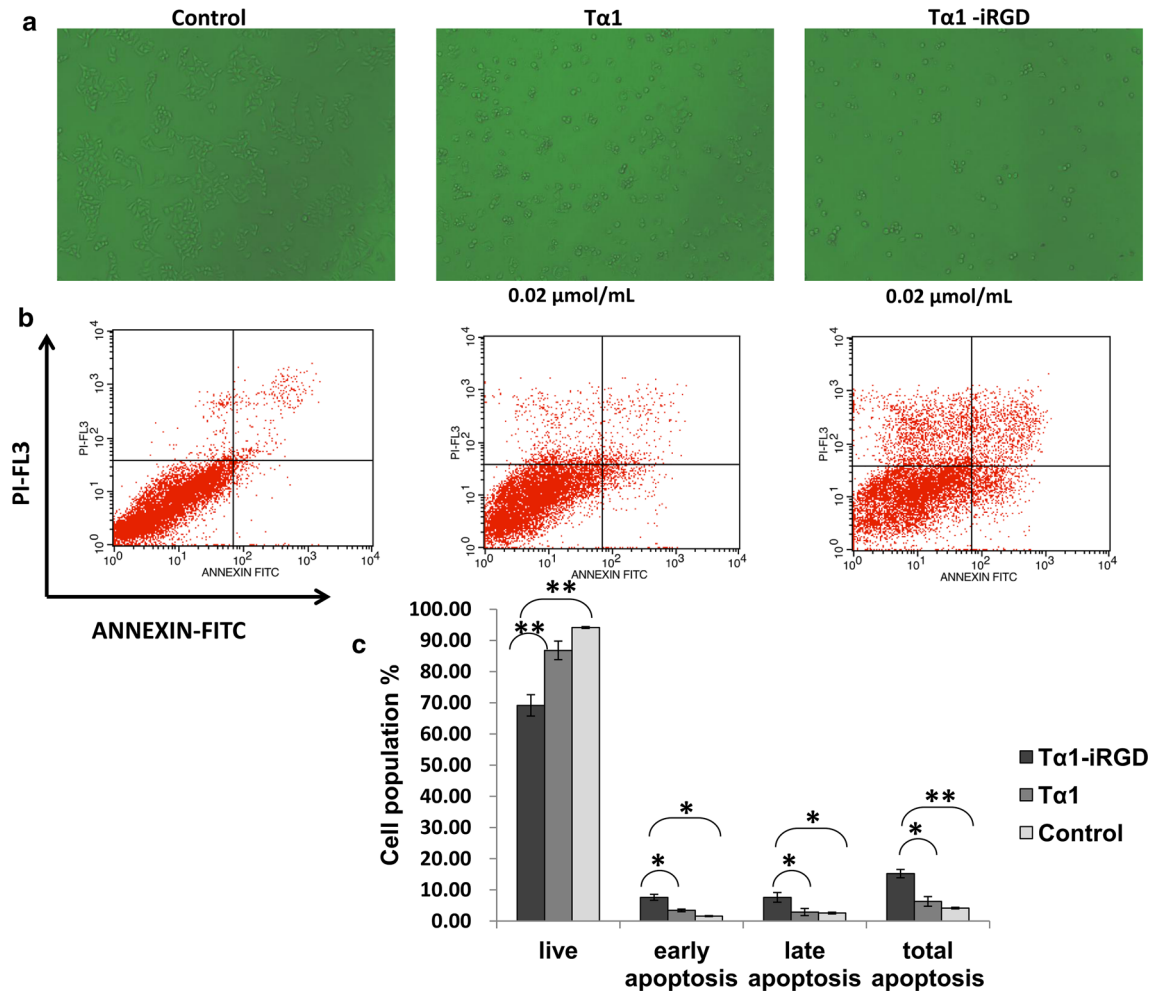

Fig. 4 Tα1-iRGD induced a more powerful effect on apoptosis than Tα1 in MCF-7 cells. **a** Morphological changes in MCF-7 cells treated with 0.02 μmol/mL Tα1-iRGD or Tα1. **b** Assessment of apoptosis induced by Tα1-iRGD or Tα1 at the concentration of 0.02 μmol/mL via Annexin V-FITC/PI staining. **c** The percentage of cells undergoing early and late apoptosis following Tα1-iRGD treatment and Tα1 treatment was compared. All data are expressed as the mean ± SD, n = 4. Statistical analyses were performed with Student's *t* test, *n.s.* not significant; *p < 0.05; **p < 0.01; ***p < 0.001

group, Tα1-iRGD treatment causes more severe tissue necrosis. Though necrosis interspersed with viable tumor cells was detected in the negative control and Tα1 treatment groups, Tα1-iRGD resulted in a large region of continuous necrosis in tumors. Vascular structures in the tumor tissues were examined using immunohistochemical staining of CD31. As shown in Fig. 8b, a decrease in the CD31 level was detected after Tα1-iRGD treatment, indicating that Tα1-iRGD exerted better effects than Tα1 on decreasing the generation of vascular structures in the tumor tissues in vivo. The further quantitative analysis showed that the administration of Ta1-iRGD decreased CD31-positive areas within the tumor by 33 % and Ta1 only by 7 %. Consistent with these results, the adding of iRGD to doxorubicin, a well-known anticancer drug, can significantly down-regulated the vascular density and diameter compared with control group [37].These results also partly explained the reason that Tα1-iRGD showed better effect on tumor inhibition than Tα1.

Tα1-iRGD show tumor-specific targeting in vivo

The specificity of the Tα1-iRGD or Tα1 in vivo was evaluated in the MCF-7 tumor-bearing models in nude mice. In brief, Tα1-iRGD or Tα1 was injected into mice via the tail vein. 2 h later, the mice were sacrificed and the tumors and other key organs were observed with in vivo imaging system. As showed in Fig. 9, only liver and kidney from both Tα1-iRGD and Tα1 groups displayed weak fluorescence signal, indicating the metabolism or secretion of peptides by these organs. More green fluorescence signal was observed in tumors of Tα1-iRGD groups than that of Tα1 groups. The further quantitative analysis showed that the administration of Ta1-iRGD resulted in a fivefold

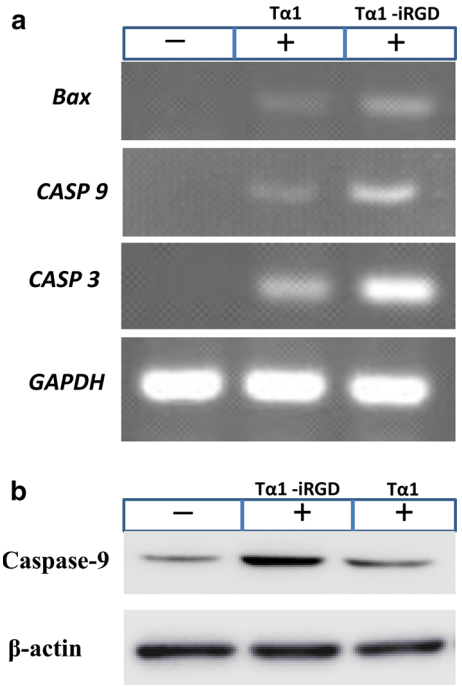

Fig. 5 RT-PCR analysis of gene expression and Western blot analysis after treatment with Tα1-iRGD or Tα1. **a** Amplified gene products were separated on 2.0 % agarose, using *GAPDH* as the internal control. The intensities of the cDNA bands for each treatment were normalised to *GAPDH* band intensities. **b** Western blot analysis

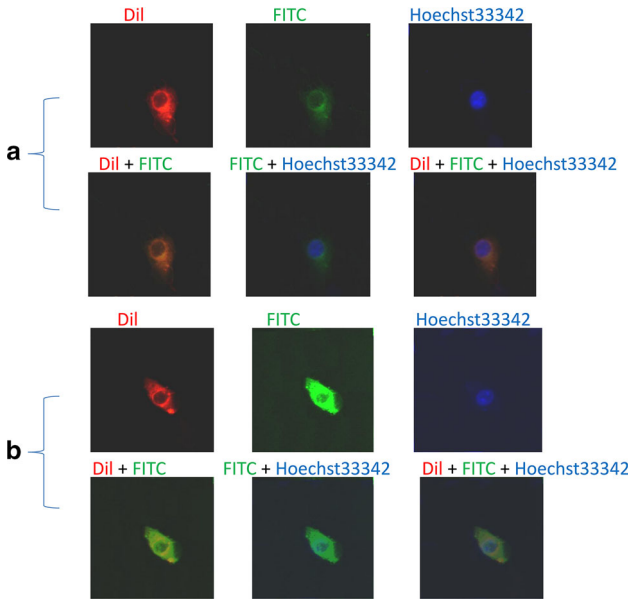

Fig. 6 Ta1-iRGD penetrate cells Distribution of Ta1-iRGD or Ta1 in cells. **a** Tα1. **b** Tα1-iRGD The fluorescein isothiocyanate-labeled peptides were showed as *green* and Hoechst33342 was used to strain the cell and showed as *blue*. Dil was used to stain the cell membrane and showed as *red*. The cyan colour represents the colocalization of peptides and nuclei. The cells were observed using inverted fluorescence microscope and their images were captured at ×400 magnification (Color figure online)

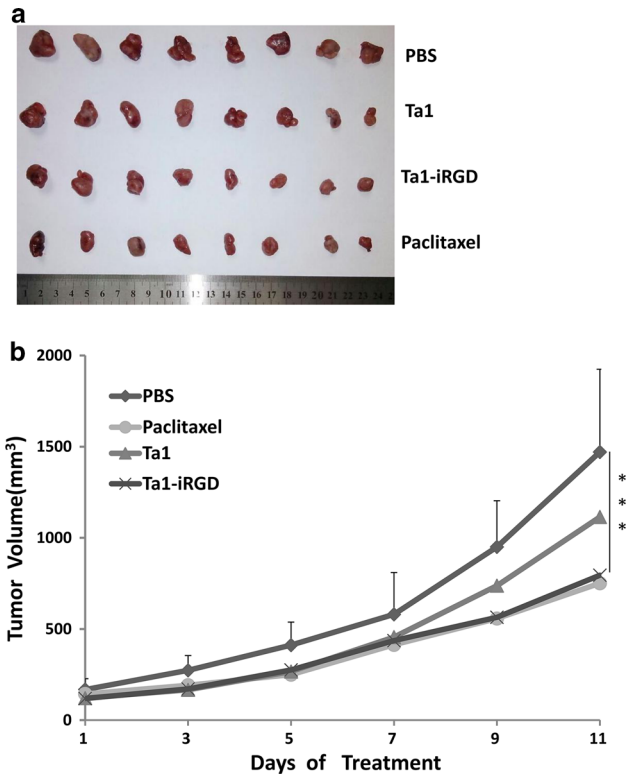

Fig. 7 The adding of iRGD enhances antitumor efficacy of Ta1. **a** Isolated tumors in different treatment group's **b** mice bearing breast cancer MCF-7 tumors were treated every day with PBS or Ta1-iRGD or Ta1. The 10 mg/kg of paclitaxel was used as positive control and s.c. administrated every 3 days. Tumor growth was evaluated every other day. Statistical significance was determined using *t* test; *n.s.* not significant;*$p < 0.05$; **$p < 0.01$; ***$p < 0.001$

increase within the tumor in the mice. It indicated that Tα1-iRGD are capable of specifically tumor-specific targeting in vivo, further confirming that iRGD is capable of delivering drug to tumors.

3D modeling

We used computational modelling to illustrate the potential reason for the improved activity of Tα1 following conjugation with iRGD. Examination of the 3D structure of both Tα1 and Tα1-CRGDK (Fig. 10a, b) demonstrated a structural resemblance between the two peptides. These models implicated that addition of iRGD or the pentapeptide CRGDK may not significantly influence the structure. The models may also be used to theoretically explain why Tα1 and Tα1-iRGD displayed similar spleen lymphocyte proliferation capability.

Previous studies have shown that iRGD is specifically recognised by αv integrins [12, 13, 16]; in addition, the pentapeptide CRGDK (a CendR peptide), which is cleaved and generated from iRGD, can readily internalise and

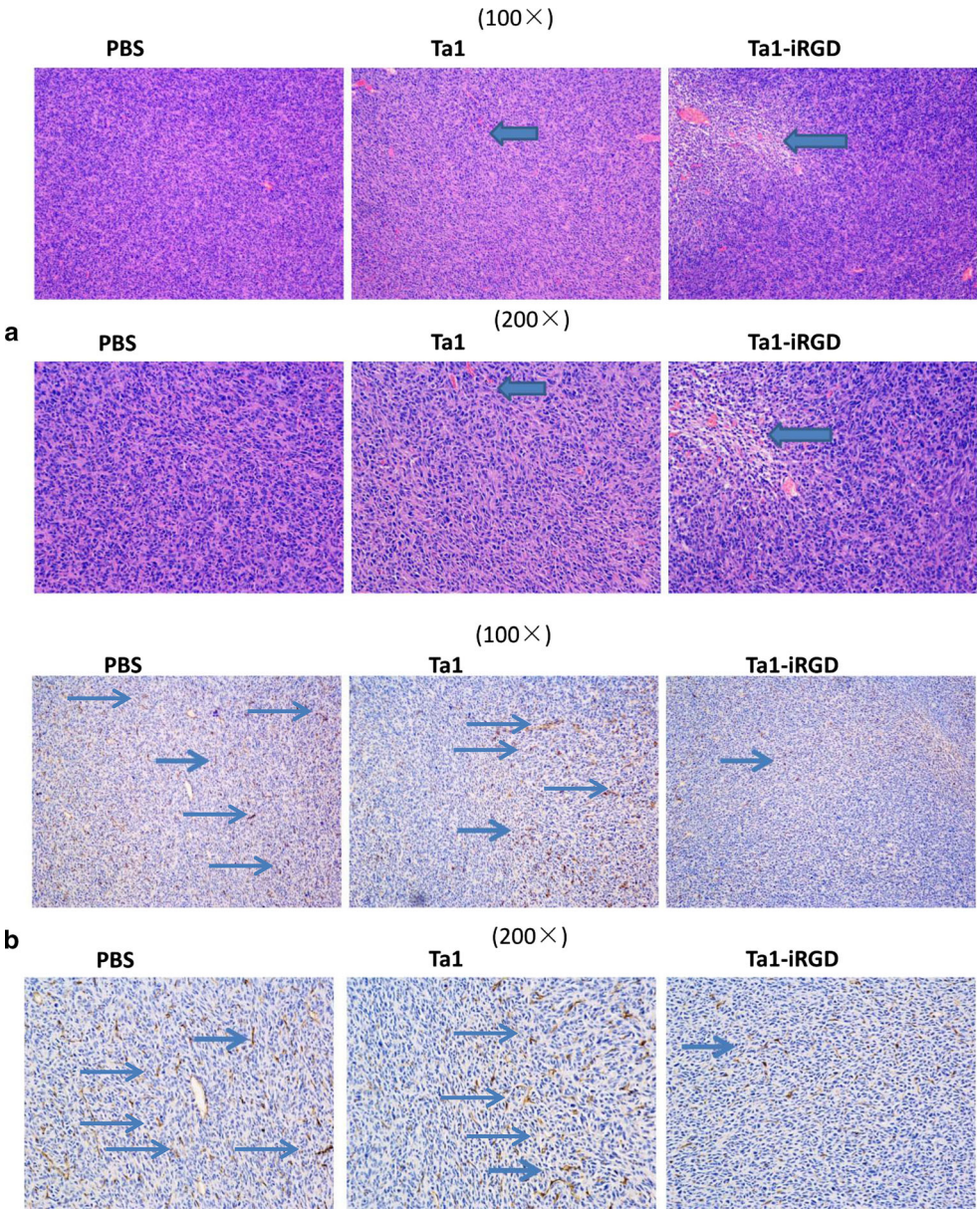

Fig. 8 Histochemistry and immunohistochemistry **a** HE staining of tumor tissues. Regions containing a large number of normal tumor cells are *dyed dark blue* and necrotic areas are *dyed pink*. The *arrows* show necrotic areas in tumor tissues. Images were captured at ×100 and ×200 magnification. **b** Immunohistochemistry to CD31 in tumor tissues. Immunohistochemistry staining of CD31was showed as *dark red* in tumors tissues. The *arrows* show blood vessels in CD31 staining in tumor tissues. Images were captured at ×100 and ×200 magnification (Color figure online)

penetrate the tumor. Several reports had proved that the CendR peptide can bind the B1 domain of NRP-1 and induce cellular internalisation and penetration [12, 16, 17, 38]. Thus, we further investigated the interaction between Tα1-CRGDK and the B1 domain of NRP-1 using a computational modelling approach. The 3D structure of the B1 domain of NRP-1 (PDB:3I97) was used as the receptor model in our Dock research.

As shown in Fig. 10c, the CRGDK part of Tα1-CRGDK could bind NRP-1 in our dock model by a mechanism similar to a small ligand binding to NRP-1 (PDB:3I97) and VEGF-A binding to NRP-1 (PDB:4DEQ). As shown in Fig. 10d, the interaction between the CRGDK part of Tα1-CRGDK and the B1 domain of NRP-1 primarily involves Tyr25, Ser26, Asn41, Asp48, Ser74 and Tyr81. The Lys side chain in Tα1-CRGDK was identified to form 2 hydrogen bonds with Asp48 and Tyr25 in our model, similar to the guanidinopentanoic acid group of the small ligand binding to NRP-1 (PDB:3I97), or the C-terminal Arg of VEGF-A binding to NRP-1 (PDB:4DEQ). Therefore, our model indicated that the C-terminal Lys of Tα1-CRGDK, which anchors in the binding pocket, plays a crucial role in binding to NRP-1 via CendR. Although computational simulation may have its own limitations in manifesting real protein–ligand interaction in detail, it is an important tool for illustrating the phenomenon observed from experiments and is useful for investigating the potential mechanism underlying the improved activity of Tα1-iRGD.

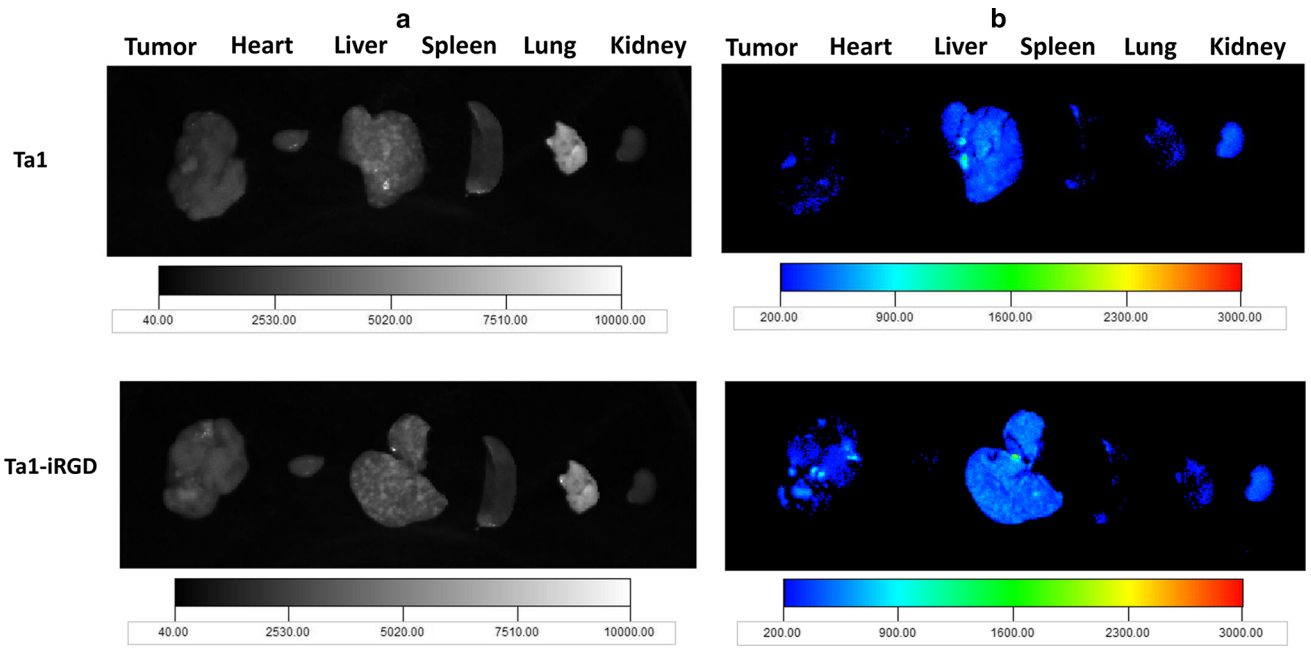

Fig. 9 Distribution of Ta1-iRGD or Ta1 in organs and tumor after tail-vein injection. **a** The tumors and organs from mice models before detection with in vivo imaging system. **b** The *green fluorescence signal* of the tumors and organs from mice models were detected under in vivo imaging system 2 h after tail-vein injection. Only liver and kidney from both Ta1-iRGD and Ta1 groups displayed weak fluorescence signal. More *green fluorescence signal* was observed in tumors of Ta1-iRGD groups than that of Ta1 groups (Color figure online)

Therefore, our model helped propose the mechanism of action underlying Tα1-CRGDK binding to NRP-1. These computational models could emphasise that adding iRGD to Tα1 may have enabled the novel function of binding to NRP-1, thus leading to cellular internalisation and penetration.

Discussion

Tα1 has confirmed its role in the stimulation of innate and adaptive immune responses under different conditions of immune suppression [5, 39–41]. Moreover, several studies have reported that Tα1 is capable of down-regulating the growth of cancer cells, such as murine B16 melanoma [42], lung cancer [43–45] and breast cancer [45]. However, the effect of Tα1 is pleiotropic, and it is usually used in combination with cytokines and chemotherapeutic agents in the treatment of cancers. Increasing the tumor-homing effect of Tα1 without altering its immune effect at the same time would generate an ideal agent for broadening the efficacy of Tα1 in cancer therapy.

In the present study, we observed that compared with Tα1, Tα1-iRGD had a significantly higher antiproliferative activity in MCF-7 breast cancer cells. Tα1-iRGD exhibited the out-standing effect in significantly inhibiting the growth of MCF-7 cells. Furthermore, the immune activities of Tα1-iRGD were also evaluated by mouse spleen lymphocyte proliferation test by co-simulating with ConA, and Tα1-iRGD showed a similar immunoregulatory effect in this assay. Tα1-iRGD had an improved capacity over Tα1 in adhering to tumor cells when evaluated by a cell attachment assay, which could partially explain the improved antiproliferative activity of Tα1-iRGD. The result of FITC-label peptides experiment in vitro also indicated that Tα1-iRGD are capable of penetrating into cells, which also could help to explain the enhancement of antitumor activity of Tα1-iRGD.

Previous studies have shown that the iRGD motif possesses tumor-homing activity by binding with αv integrins that are up-regulated in certain tumor cells [14, 46]. The iRGD motif in turn is cleaved by a protease to generate a CendR peptide (K/RXXK/R), which can promote binding and internalisation into tumor cells [12, 16]. Based on these studies, Tα1-iRGD should be cleaved into Tα1-CRGDK, which also contains a CendR peptide. To illustrate whether Tα1-CRGDK can bind NRP-1 [31], we employed computational simulation methods to successfully build a binding model of Tα1-CRGDK and NRP-1. Because the binding of a CendR peptide to NRP-1 has been proven to play a crucial rule in cellular internalisation and penetration [16, 47], the specific interactions found in the Tα1-CRGDK-NRP-1 complex from our virtual models suggested that Tα1-iRGD was far superior to Tα1 in inhibiting the growth of tumor cells.

We also observed morphological alterations in MCF-7 cells following a 36 h treatment during the MTT assay,

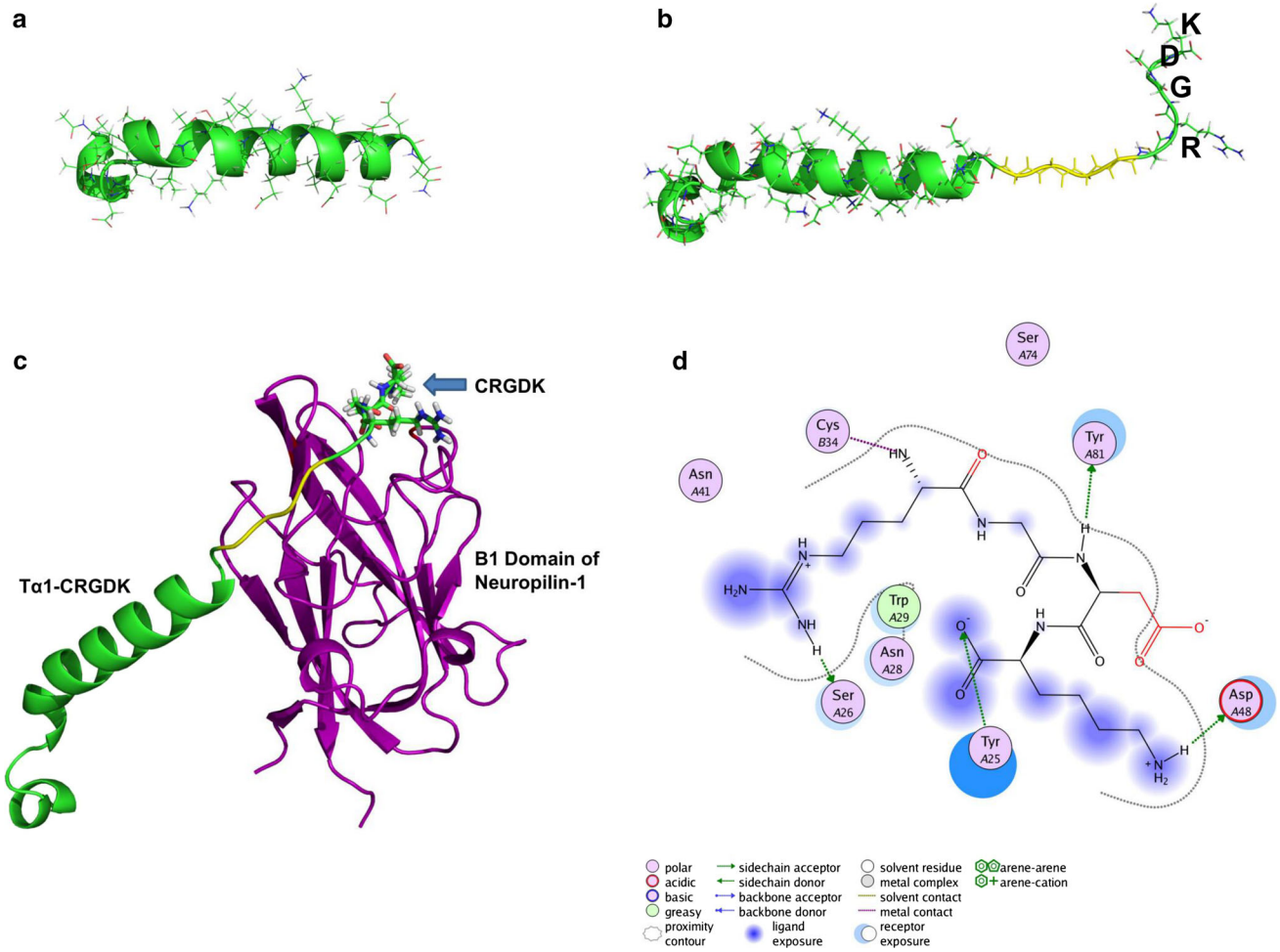

Fig. 10 Modeling of the structures of Tα1-CRGDK and NRP-1 complexed with Tα1-CRGDK. **a** Tα1. Tα1 is shown in *green*. **b** Tα1-CRGDK. The Tα1 part of Tα1-iRGD is shown in *green*, the CRGDK part is shown as a line in *green* and the linker between them is shown in *yellow*. **c** Schematic illustration of the model of the NRP-1-Tα1-CRGDK complex. NRP-1 is shown in *purple* and Tα1-CRGDK in green (the linker is shown in *yellow*). **d** Focused view of the binding site. Specific interactions between the CRGDK part of Tα1-CRGDK and NRP-1 are drawn. Hydrogen bonds are shown as *green discontinuous lines*. The NRP-1-Tα1-CRGDK structure reveals that the CRGDK part of Tα1-CRGDK can bind NRP-1 in a manner similar to the interaction between NRP-1 and a small ligand that contains a guanidinopentanoic acid group (PDB:3I97) (Color figure online)

such as cell shrinkage, which is one of the characteristics of apoptosis. The result of apoptosis analysis showed that Tα1-iRGD induced a better effect on simulating cell apoptosis than Tα1 in MCF-7 cells. Although other research groups have previously assessed the role of Tα1 in inducing apoptosis in human leukaemia cells [48], this is the first study, to our knowledge, to compare the effect of Tα1-iRGD and Tα1 on the induction of apoptosis in MCF-7 cells. Induction of apoptosis is one of the most important attributes of tumor suppression [49–51]. Thus, we explored the potential effect of Tα1-iRGD or Tα1 in apoptosis signalling in MCF-7 cells. *Bax* is usually believed to be an extremely important factor that can trigger apoptosis; thus a direct induction of *Bax* is considered an attractive strategy for treating cancer [32]. Therefore, to investigate why Tα1-iRGD was more effective in inducing cell apoptosis than Tα1 in MCF-7 cells, we studied the changes in expression of apoptosis-associated genes by semi-quantitative RT-PCR. We observed that the expression of *Bax*, *CASP9* and *CASP3* were all significantly higher in Tα1-iRGD-treated MCF-7 cells than in Tα1-treated cells. This suggests that both Tα1 and Tα1-iRGD are involved in the mitochondria-mediated apoptosis pathway, although Tα1-iRGD is more effective in inducing apoptosis of MCF-7 cells.

Subsequent injections of Tα1-iRGD inhibited MCF-7 breast tumor progression more efficiently than the native Ta1 in vivo. To find out whether the induction of tumor-specific responses would contribute to the antitumor effects observed, we also analyzed the expression of CD31 in tumor tissues by immunohistochemistry and the tumor-homing effect by FITC-labelling assay. Significantly less

levels of CD31 were observed when tumor-bearing mice were treated with Tα1-iRGD compared with Tα1. Furthermore, Tα1-iRGD also showed tumor-specific targeting in vivo, but Tα1 showed not any the same feature. These findings highlight the importance of iRGD on enhancement of tumor accumulation, suggesting that the adding of iRGD could remarkably improve the efficacy of Tα1 on tumor therapy.

Conclusion

Collectively, our results demonstrated that addition of iRGD to Tα1 significantly enhanced the basal ability of Tα1 to inhibit proliferation of MCF-7 cells in vitro and antitumor effect in vivo. Our findings further indicated that the addition of the iRGD fragment increased the antiproliferative activity of Tα1 against breast cancer cells by improving the ability of Tα1 to attach and penetrate tumor cells, in addition to an improved effect in *Bax*-induced mitochondria-mediated apoptosis in MCF-7 cells. The antiproliferative activity of Tα1-iRGD reinforces its potential use as a promising and novel modified inhibitor of breast cancer.

Acknowledgments The authors would like to thank Dr. Jing Li for the discussions and helpful suggestions during this investigation. This work was supported by the National Natural Science Foundation of China (Grant No. 31300643) and a grant from the National High Technology Research and Development Program of China (863) (No. 2012AA020304) and the Fundamental Research Funds for the Central Universities (PT2014SK0062).

References

1. Goldstein AL, Low TL, McAdoo M, McClure J, Thurman GB et al (1977) Thymosin alpha1: isolation and sequence analysis of an immunologically active thymic polypeptide. Proc Natl Acad Sci USA 74:725–729
2. Hadden JW (2003) Immunodeficiency and cancer: prospects for correction. Int Immunopharmacol 3:1061–1071
3. Leung N (2002) Treatment of chronic hepatitis B: case selection and duration of therapy. J Gastroenterol Hepatol 17:409–414
4. Chadwick D, Pido-Lopez J, Pires A, Imami N, Gotch F et al (2003) A pilot study of the safety and efficacy of thymosin alpha 1 in augmenting immune reconstitution in HIV-infected patients with low CD4 counts taking highly active antiretroviral therapy. Clin Exp Immunol 134:477–481
5. Goldstein AL, Goldstein AL (2009) From lab to bedside: emerging clinical applications of thymosin alpha 1. Expert Opin Biol Ther 9:593–608
6. Danielli R, Fonsatti E, Calabro L, Di Giacomo AM, Maio M (2012) Thymosin alpha1 in melanoma: from the clinical trial setting to the daily practice and beyond. Ann N Y Acad Sci 1270:8–12
7. Garaci E, Pica F, Rasi G, Favalli C (2000) Thymosin alpha 1 in the treatment of cancer: from basic research to clinical application. Int J Immunopharmacol 22:1067–1076
8. Garaci E, Pica F, Sinibaldi-Vallebona P, Pierimarchi P, Mastino A et al (2003) Thymosin alpha(1) in combination with cytokines and chemotherapy for the treatment of cancer. Int Immunopharmacol 3:1145–1150
9. Garaci E, Lopez M, Bonsignore G, Della Giulia M, D'Aprile M et al (1995) Sequential chemoimmunotherapy for advanced non-small cell lung cancer using cisplatin, etoposide, thymosin-alpha 1 and interferon-alpha 2a. Eur J Cancer 31A:2403–2405
10. Lopez M, Carpano S, Cavaliere R, Di Lauro L, Ameglio F et al (1994) Biochemotherapy with thymosin alpha 1, interleukin-2 and dacarbazine in patients with metastatic melanoma: clinical and immunological effects. Ann Oncol 5:741–746
11. Bepler G (1994) Thymosin alpha-1 as adjunct for conventional therapy of malignant-tumors—a review. Cancer Investig 12:491–496
12. Sugahara KN, Teesalu T, Karmali PP, Kotamraju VR, Agemy L et al (2009) Tissue-penetrating delivery of compounds and nanoparticles into tumors. Cancer Cell 16:510–520
13. Sugahara KN, Teesalu T, Karmali PP, Kotamraju VR, Agemy L et al (2010) Coadministration of a tumor-penetrating peptide enhances the efficacy of cancer drugs. Science 328:1031–1035
14. Ruoslahti E (2002) Specialization of tumour vasculature. Nat Rev Cancer 2:83–90
15. Desgrosellier JS, Cheresh DA (2010) Integrins in cancer: biological implications and therapeutic opportunities. Nat Rev Cancer 10:9–22
16. Teesalu T, Sugahara KN, Kotamraju VR, Ruoslahti E (2009) C-end rule peptides mediate neuropilin-1-dependent cell, vascular, and tissue penetration. Proc Natl Acad Sci USA 106:16157–16162
17. Roth L, Agemy L, Kotamraju VR, Braun G, Teesalu T et al (2012) Transtumoral targeting enabled by a novel neuropilin-binding peptide. Oncogene 31:3754–3763
18. Lao X, Liu M, Chen J, Zheng H (2013) A tumor-penetrating Peptide modification enhances the antitumor activity of thymosin alpha 1. PLoS One 8:e72242
19. Carmichael J, DeGraff WG, Gazdar AF, Minna JD, Mitchell JB (1987) Evaluation of a tetrazolium-based semiautomated colorimetric assay: assessment of chemosensitivity testing. Cancer Res 47:936–942
20. Wang P, Ballestrem C, Streuli CH (2011) The C terminus of talin links integrins to cell cycle progression. J Cell Biol 195:499–513
21. Wang J, Chen B, Jin N, Xia G, Chen Y et al (2011) The changes of T lymphocytes and cytokines in ICR mice fed with Fe3O4 magnetic nanoparticles. Int J Nanomed 6:605–610
22. Rossi A, Lord JM (2013) Adiponectin inhibits neutrophil apoptosis via activation of AMP kinase, PKB and ERK 1/2 MAP kinase. Apoptosis 18:1469–1480
23. Vermes I, Haanen C, Steffens-Nakken H, Reutelingsperger C (1995) A novel assay for apoptosis. Flow cytometric detection of phosphatidylserine expression on early apoptotic cells using fluorescein labelled Annexin V. J Immunol Methods 184:39–51
24. Shetty J, Klotz KL, Wolkowicz MJ, Flickinger CJ, Herr JC (2007) Radial spoke protein 44 (human meichroacidin) is an axonemal alloantigen of sperm and cilia. Gene 396:93–107
25. Xu HM, Yin R, Chen L, Siraj S, Huang X et al (2008) An RGD-modified endostatin-derived synthetic peptide shows antitumor activity in vivo. Bioconjug Chem 19:1980–1986
26. Yang W, Luo D, Wang S, Wang R, Chen R et al (2008) TMTP1, a novel tumor-homing peptide specifically targeting metastasis. Clin Cancer Res 14:5494–5502
27. Elizondo-Riojas MA, Chamow SM, Tuthill CW, Gorenstein DG, Volk DE (2011) NMR structure of human thymosin alpha-1. Biochem Biophys Res Commun 416:356–361
28. Jarvis A, Allerston CK, Jia H, Herzog B, Garza-Garcia A et al (2010) Small molecule inhibitors of the neuropilin-1 vascular

endothelial growth factor A (VEGF-A) interaction. J Med Chem 53:2215–2226
29. Chen R, Li L, Weng Z (2003) ZDOCK: an initial-stage protein-docking algorithm. Proteins 52:80–87
30. Vintonenko N, Pelaez-Garavito I, Buteau-Lozano H, Toullec A, Lidereau R et al (2011) Overexpression of VEGF189 in breast cancer cells induces apoptosis via NRP1 under stress conditions. Cell Adhes Migr 5:332–343
31. Jubb AM, Strickland LA, Liu SD, Mak J, Schmidt M et al (2012) Neuropilin-1 expression in cancer and development. J Pathol 226:50–60
32. Wei MC, Zong WX, Cheng EH, Lindsten T, Panoutsakopoulou V et al (2001) Proapoptotic BAX and BAK: a requisite gateway to mitochondrial dysfunction and death. Science 292:727–730
33. Riedl SJ, Salvesen GS (2007) The apoptosome: signalling platform of cell death. Nat Rev Mol Cell Biol 8:405–413
34. Li P, Nijhawan D, Budihardjo I, Srinivasula SM, Ahmad M et al (1997) Cytochrome c and dATP-dependent formation of Apaf-1/caspase-9 complex initiates an apoptotic protease cascade. Cell 91:479–489
35. Cepero E, King AM, Coffey LM, Perez RG, Boise LH (2005) Caspase-9 and effector caspases have sequential and distinct effects on mitochondria. Oncogene 24:6354–6366
36. Brentnall M, Rodriguez-Menocal L, De Guevara RL, Cepero E, Boise LH (2013) Caspase-9, caspase-3 and caspase-7 have distinct roles during intrinsic apoptosis. BMC Cell Biol 14:32
37. Wang K, Zhang XF, Liu Y, Liu C, Jiang BH et al (2014) Tumor penetrability and anti-angiogenesis using iRGD-mediated delivery of doxorubicin-polymer conjugates. Biomaterials 35: 8735–8747
38. Becker PM, Waltenberger J, Yachechko R, Mirzapoiazova T, Sham JS et al (2005) Neuropilin-1 regulates vascular endothelial growth factor-mediated endothelial permeability. Circ Res 96:1257–1265
39. Romani L, Bistoni F, Gaziano R, Bozza S, Montagnoli C et al (2004) Thymosin alpha 1 activates dendritic cells for antifungal Th1 resistance through toll-like receptor signaling. Blood 103:4232–4239
40. Leichtling KD, Serrate SA, Sztein MB (1990) Thymosin alpha 1 modulates the expression of high affinity interleukin-2 receptors on normal human lymphocytes. Int J Immunopharmacol 12:19–29
41. Garaci E, Pica F, Serafino A, Balestrieri E, Matteucci C et al (2012) Thymosin alpha1 and cancer: action on immune effector and tumor target cells. Ann N Y Acad Sci 1269:26–33
42. Pica F, Fraschetti M, Matteucci C, Tuthill C, Rasi G (1998) High doses of thymosin alpha 1 enhance the anti-tumor efficacy of combination chemo-immunotherapy for murine B16 melanoma. Anticancer Res 18:3571–3578
43. Moody TW, Fagarasan M, Zia F, Cesnjaj M, Goldstein AL (1993) Thymosin alpha 1 down-regulates the growth of human non-small cell lung cancer cells in vitro and in vivo. Cancer Res 53:5214–5218
44. Mastino A, Favalli C, Grelli S, Rasi G, Pica F et al (1992) Combination therapy with thymosin alpha 1 potentiates the anti-tumor activity of interleukin-2 with cyclophosphamide in the treatment of the Lewis lung carcinoma in mice. Int J Cancer 50:493–499
45. Moody TW (2007) Thymosin alpha1 as a chemopreventive agent in lung and breast cancer. Ann N Y Acad Sci 1112:297–304
46. Eliceiri BP, Cheresh DA (2001) Adhesion events in angiogenesis. Curr Opin Cell Biol 13:563–568
47. Parker MW, Xu P, Li X, Vander Kooi CW (2012) Structural basis for selective vascular endothelial growth factor-A (VEGF-A) binding to neuropilin-1. J Biol Chem 287:11082–11089
48. Fan YZ, Chang H, Yu Y, Liu J, Wang R (2006) Thymosin alpha1 suppresses proliferation and induces apoptosis in human leukemia cell lines. Peptides 27:2165–2173
49. Panchal RG (1998) Novel therapeutic strategies to selectively kill cancer cells. Biochem Pharmacol 55:247–252
50. Schwartz GK, Shah MA (2005) Targeting the cell cycle: a new approach to cancer therapy. J Clin Oncol 23:9408–9421
51. Elmore S (2007) Apoptosis: a review of programmed cell death. Toxicol Pathol 35:495–516